Variable Rainfall over Steady SST: The Effect of the Free Troposphere on Surface Pressure in the East Pacific

ISABELLE BUNGE,[a] ADAM SOBEL,[a,b] MICHELA BIASUTTI,[b] AND SHUGUANG WANG[c]

[a] *Department of Applied Physics and Applied Mathematics, Columbia University, New York, New York*
[b] *Lamont-Doherty Earth Observatory, Columbia University, Palisades, New York*
[c] *School of Atmospheric Sciences, Nanjing University, Nanjing, China*

(Manuscript received 2 June 2023, in final form 3 October 2023, accepted 13 October 2023)

ABSTRACT: Surface winds and precipitation over the tropical oceans are related to sea surface temperature (SST) through multiple mechanisms. Greater SST is associated with greater conditional instability, which in turn is more conducive to deep convection. The associated mass and flow responses can extend to the surface, via associated pressure gradients imprinted on the top of the planetary boundary layer (PBL). SST also influences surface pressure and wind directly through its control over PBL temperature, as explained by Lindzen and Nigam. The authors examine the relative magnitudes of these two influences over the eastern tropical Pacific on subseasonal precipitation variability during northern summer, when and where SST gradients are largest and the direct influence via PBL temperature is expected to be strongest. Geopotential at 1000 hPa is partitioned into two components: the geopotential at the PBL top (the PBL top is chosen to be 850 hPa, supported by an analysis of the vertical structure of geopotential and temperature) and the PBL thickness. These fields are composited on quintiles of daily ITCZ precipitation both with and without a high-pass filter that isolates subseasonal time scales. The PBL thickness varies little between the highest and lowest precipitation quintiles, while the PBL top geopotential varies much more. This supports a view in which the direct contribution of SST to the surface pressure and flow fields, including the associated PBL convergence over sharp SST maxima, can be viewed as a steady forcing on the rest of the column, while free-tropospheric transients contribute most of the variability associated with precipitation on subseasonal time scales.

KEYWORDS: Pacific Ocean; Tropics; Boundary layer; Rainfall; Sea surface temperature; Atmospheric waves

1. Introduction

There is a strong spatial coincidence between sea surface temperature (SST) and precipitation in the tropics, particularly on seasonal and longer time scales. Regions of high SST tend to be rainy, while regions of low SST tend to be dry (Bjerknes 1969). Yet the mechanisms behind this relationship remain in some respects less than entirely clear because more than one mechanism appears able to explain it (e.g., Sobel 2007).

Near-surface temperature and humidity are largely controlled by SST. But the free-tropospheric temperature profile must be similar in regions of higher and lower SST, due to the weakness of free-tropospheric temperature gradients, in turn a consequence of the small Coriolis parameter near the equator. Thus, the atmosphere above low SST is generally unconditionally stable to deep convection, with a cool boundary layer separated from a warm troposphere by an inversion, while the atmosphere above high SST is generally conditionally unstable and, all else equal, prone to deep convection. This explanation for the close relationship between SST and precipitation in the tropics can be captured economically with a single-column model under the weak temperature gradient (WTG) approximation, given the SST and free-tropospheric temperature profile as inputs (e.g., Sobel and Bretherton 2000; Daleu et al. 2015, 2016).

The above argument also predicts low-level wind convergence over high SST, since the precipitation is associated with diabatic heating and ascent in the free troposphere and these must be balanced by mass and moisture convergence below. The convergence in this view is a by-product of the precipitation, rather than an independent cause of it. The rotational wind and surface pressure field must also be related to the convergence (or more generally to the wind) so as to satisfy the momentum budget (Held and Hoskins 1985; Sobel et al. 2001), but in this view that is yet one step further down the causal chain that begins with column stability. The connection between tropospheric heating, surface wind, and pressure is often interpreted through linear shallow-water models (Matsuno 1966; Webster 1972; Gill 1980).

In the above WTG view, SST controls deep convection first, and surface wind is a by-product. On the other hand, SST gradients can also influence winds in the planetary boundary layer (PBL) directly, as originally articulated by Lindzen and Nigam (1987, hereafter LN87) and subsequently extended and improved by Battisti et al. (1999). The PBL air temperature adjusts toward the SST through sensible heat flux. Under hydrostatic balance, the surface pressure field then has a component that is directly related to the SST, with low pressure over high SST and high pressure over low SST. LN87 neglected horizontal pressure gradients above the PBL

Supplemental information related to this paper is available at the Journals Online website: https://doi.org/10.1175/JAS-D-23-0101.s1.

Corresponding author: Isabelle Bunge, ieb2123@columbia.edu

DOI: 10.1175/JAS-D-23-0101.1

top, so that spatial variations in surface pressure are solely a consequence of PBL temperature variations and thus of SST variations (since those control PBL temperature) due to this mechanism.

Given the surface pressure field, surface and PBL winds follow from the pressure via Ekman layer dynamics, modified to account for exchange of mass and momentum with the free troposphere (LN87; also Battisti et al. 1999; Chiang et al. 2001; Stevens et al. 2002; McGauley et al. 2004; Raymond et al. 2006; Back and Bretherton 2009a, hereafter BB09a; Duffy et al. 2020). Where surface winds converge, moisture does also, since the PBL over low-latitude oceans is invariably humid. Conservation of mass requires ascent at PBL top, and this ascent will invariably be associated with convective clouds. Under some further assumptions—particularly that the ascent at PBL top extends well into the troposphere, rather than feeding a shallow return flow via divergence just above the PBL (e.g., Zhang et al. 2004)—these convective clouds result in precipitation. Thus, this model also predicts that SST and precipitation will be closely associated, but now the argument is based primarily on the momentum dynamics of the PBL, with no explicit appeal to column stability.

Each of the above views has its limitations and subtly overlaps with the other. Here, we focus on just a subset of the issues; others are discussed at length elsewhere (e.g., Neelin 1989; Battisti et al. 1999; Wu et al. 1999; Chiang et al. 2001; Sobel 2007; BB09a; Back and Bretherton 2009b). For our purpose, the most important limitation of LN87 is its neglect of free-tropospheric pressure gradients. LN87 compensate by defining the PBL top to be at 700 hPa, arguably incorporating some of what is really the free troposphere. Meanwhile, the most important limitation of the WTG view is its neglect of any PBL convergence directly driven by SST gradients as in LN87. Under WTG, all that matters is the difference between the local SST and the tropical mean SST, or whatever statistic of the SST field (e.g., the SST of the rainiest regions; cf. Sobel et al. 2002; Fueglistaler and Silvers 2021) controls the tropospheric temperature. The particular spatial structure of the SST field is irrelevant under WTG; yet in reality, a sufficiently narrow SST maximum is different than a broad one. Strong hydrostatic PBL pressure gradients around a narrow one can provide additional convergence that acts as an additional forcing on deep convection (Sobel and Neelin 2006; BB09a).

These issues come into particularly strong focus in the eastern tropical Pacific, since SST gradients are particularly large there. Chiang et al. (2001) systematically and carefully evaluated the importance of the pressure gradient in the PBL associated directly with SST (i.e., the LN87 effect), compared to that of free-tropospheric heating, in determining the surface wind, and found that the former is more important in the eastern Pacific than anywhere else, specifically for determining the meridional wind. Free-tropospheric heating here presumably affects the surface wind through free-tropospheric pressure gradients that impose themselves on the PBL from above, gradients that LN87 neglect. Broadly consistent with this, BB09a used an atmospheric mixed-layer model to show that zonal surface winds are primarily set by the free-tropospheric pressure gradients (themselves presumably influenced by free-tropospheric heating) as well as downward momentum mixing, while the climatological surface convergence is set directly by the underlying SST gradients.

Besides the surface wind, these issues are relevant to the vertical structure of the tropospheric flow. Indeed, building on BB09a, Back and Bretherton (2009b) constructed an idealized model with two vertical modes to predict precipitation and vertical motion from the SST field, considering the shallow mode to be directly related to SST-controlled PBL convergence and the deep mode to be related to column stability (which in turn is also influenced by SST); the top- or bottom-heaviness of the vertical motion profile in a given location depends on the relative amplitudes of the two modes. This is particularly relevant to the eastern Pacific intertropical convergence zone (ITCZ); the extent that convergence is driven by gradients in SST and PBL temperature more directly there than elsewhere, one might expect it to yield a more bottom-heavy profile of large-scale ascent and thus a small or negative gross moist stability (Back and Bretherton 2006; Sobel and Neelin 2006; Back and Bretherton 2009b). Since large-scale vertical motion is a relatively poorly observed field, it has been debated to what extent this is the case [e.g., see the introduction of Huaman et al. (2022) for further discussion and references]. Recently, Fuchs-Stone et al. (2020) and Huaman et al. (2022) examined this question using observations from the Organization of Tropical East Pacific Convection (OTREC2019) field program, which also motivated the present study.

Here, we study the surface pressure field and its relationship to precipitation in the eastern Pacific ITCZ. We focus on surface pressure (or in pressure coordinates, 1000-hPa geopotential) because it is the field most directly controlled by SST, mediating the response of surface wind and precipitation to SST, in LN87 and related studies. We ask to what extent temporal variations in the pressure field associated with temporal variations in ITCZ precipitation are determined by PBL thickness (the component most directly associated with SST, per LN87) versus imposed on the PBL from above (and presumably related to free-tropospheric dynamics).

Since PBL temperature is so tightly coupled to SST, and SST evolves slowly compared to many atmospheric transients of interest, we might hypothesize that the mass and moisture convergence related to the directly SST-controlled component of the pressure field can be considered steady for many purposes. Yet precipitation is quite unsteady. Over the eastern Pacific ITCZ in particular, there is substantial variability in precipitation on subseasonal time scales (Gonzalez et al. 2022). If this is supported by similar variability in surface pressure (and associated convergence), some of that is presumably imposed on the PBL from above. We hypothesize the following:

1) There is a component of the surface pressure gradient and low-level wind field that is driven primarily by the SST field via its control over the atmospheric temperature. This component remains nearly constant as precipitation varies.
2) Subseasonal variations in surface pressure gradient, horizontal wind in the PBL, and associated mass and moisture convergence are controlled primarily by free-tropospheric

pressure variations that are associated with variations in precipitation.

To the extent these hypotheses are correct, they imply a view in which the component of PBL convergence directly controlled by SST gradients acts as a steady forcing on ITCZ convection, but this forcing does not determine the occurrence or intensity of convection in a direct or simple way, since free-tropospheric transients also play an important role.

Besides informing our physical understanding, and assessing the strengths and limitations of various idealized models for the surface wind field over tropical oceans, we also aim to inform single-column modeling approaches using parameterization of large-scale dynamics. To the extent that the first hypothesis above is correct, the component of the convergence and associated vertical motion associated directly with SST gradients require special attention under such approaches. Bellon and Sobel (2010) constructed a WTG single-column model in which PBL convergence, assumed to be driven by SST gradients as in LN87, was imposed as an additional external forcing, but their model was highly idealized, with simple, assumed vertical structures, following the "second quasi-equilibrium tropical circulation model" (Sobel and Neelin 2006; Lintner et al. 2012). Recently, Bernardez and Back (2022) found in a simple single-column model under WTG that they were able to simulate the shallow component of vertical motion by imposing shallow atmospheric temperature variations that are in turn consequences of SST gradients, so that the latter and their associated convergence both enter implicitly through the atmospheric column stability. Further exploration of these (and perhaps other) different ways of representing these complex interactions between large-scale dynamics and column thermodynamics in SCMs should be informed by analyses like those we perform here.

As part of our analysis, we consider how best to determine the depth of the PBL itself for our purposes. Idealized models for the horizontal structure of the PBL flow, like those discussed above (Battisti et al. 1999; Chiang et al. 2001; Stevens et al. 2002; McGauley et al. 2004; Raymond et al. 2006; BB09a; Gonzalez et al. 2016), require a specification of PBL depth. Some approaches for single-column modeling using WTG or other parameterizations of large-scale dynamics also require a choice of PBL depth. In either type of idealized model—focusing on either horizontal or vertical dimensions of the flow—the choice of PBL depth can be consequential. We address this below by looking at how the horizontal variances in temperature and geopotential vary as functions of height (strictly, pressure).

We study the above issues by using observation-based and reanalysis datasets to construct composites of geopotential and wind convergence, conditioned on the precipitation in the eastern Pacific ITCZ. We work in pressure coordinates, so that geopotential plays the role that pressure would in height coordinates, and 1000-hPa geopotential plays the role of surface pressure. Section 2 describes the datasets used to study the PBL and free-tropospheric components of the 1000-hPa geopotential and the methods for the analysis. Section 3 presents the results, and some interpretation regarding the roles of the free-tropospheric and PBL thickness components of 1000-hPa geopotential on subseasonal rainfall events in the EP. Finally, section 4 presents conclusions and suggests directions for future work.

2. Data and methods

a. *Rainfall and reanalysis dataset*

We use the Tropical Rainfall Measuring Mission (TRMM) 3B42 precipitation product (Tropical Rainfall Measuring Mission 2018), defined on a 0.25° horizontal resolution grid at 3-hourly time steps between 1998 and 2019. The rainfall rates are derived from merged satellite rainfall estimates that are calibrated using monthly gauge data. For the analysis presented in this paper, rainfall rates are averaged to daily time resolution. We have also repeated our entire analysis with temporal resolutions of 6 h and 10 days, and the conclusions do not change qualitatively (a summary of which is included in the online supplemental materials). The coherence of our analysis over different temporal resolutions suggests that our conclusions apply over a broad range of subseasonal time scales.

Geopotential, temperature, and wind fields are taken from the European Centre for Medium-Range Weather Forecasts (ECMWF) ERA5 reanalysis dataset, which provides hourly data on a 0.25° horizontal resolution grid and 37 pressure levels (Hersbach et al. 2023a). These products are available from 1950 to the present, but we consider only 1998–2019 in order to match the TRMM 3B42 product. As with the latter data, the hourly ERA5 products are also averaged to daily time resolution. To determine the pressure level of the top of the PBL, monthly averaged temperature and geopotential ERA5 products from 2007 to 2017 are used (Hersbach et al. 2023b).

b. *Precipitation composites*

Rainfall events are defined over an eastern Pacific ITCZ region extending approximately 10 000 km zonally along the ITCZ (from 160° to 86°W). We have also conducted the analysis for domains of smaller zonal extents, and the results are not qualitatively sensitive to this choice (see supplementary materials).

At each longitude within the chosen longitude range, and for each 3-month season defined here, the meridional boundary of the nominal ITCZ is defined as that over which the climatological precipitation rate is greater than 0.2 mm h^{-1}. Figure 1 displays the boxes used to define the rainfall composites for each season. The daily precipitation rate is averaged spatially over the defined region and then binned into quintiles, i.e., five evenly spaced bins, where the lowest bin corresponds to days with the least precipitation and the highest bin corresponds to days with the most precipitation. A histogram of rainfall rates for each season as well as the boundaries of the quintiles is shown in Fig. 2. In the supplement, we also present results in which precipitation is averaged over 6-h and 10-day periods; these results are qualitatively similar to those shown below, such that we take the daily results as representative of a broad range of subseasonal time scales.

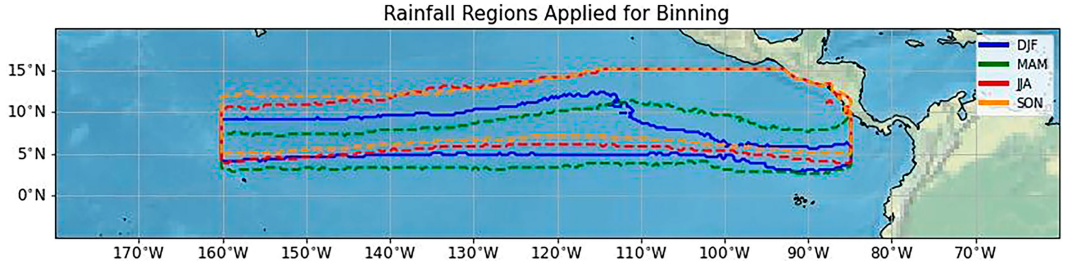

FIG. 1. Rainfall regions used for the analysis for DJF, MAM, JJA, and SON. Rainfall regions were set by taking the locations where the seasonal average of precipitation (TRMM 3B42) is greater than 5 mm day^{-1}.

c. *Geopotential decompositions*

The geopotential and temperature fields are examined in their original forms as well as under a high-pass, fifth-order Butterworth filter. The Butterworth filter used in this study selects a critical frequency of 1/96 day^{-1} and is applied to a dataset tapered along the time axis to reduce "ringing" during signal processing. The high-pass filter is designed to remove seasonal and slower signals, including those associated with the El Niño–Southern Oscillation (ENSO) phenomenon and other slow SST variability, in order to isolate subseasonal structures in geopotential that are related directly to subseasonal precipitation fluctuations.

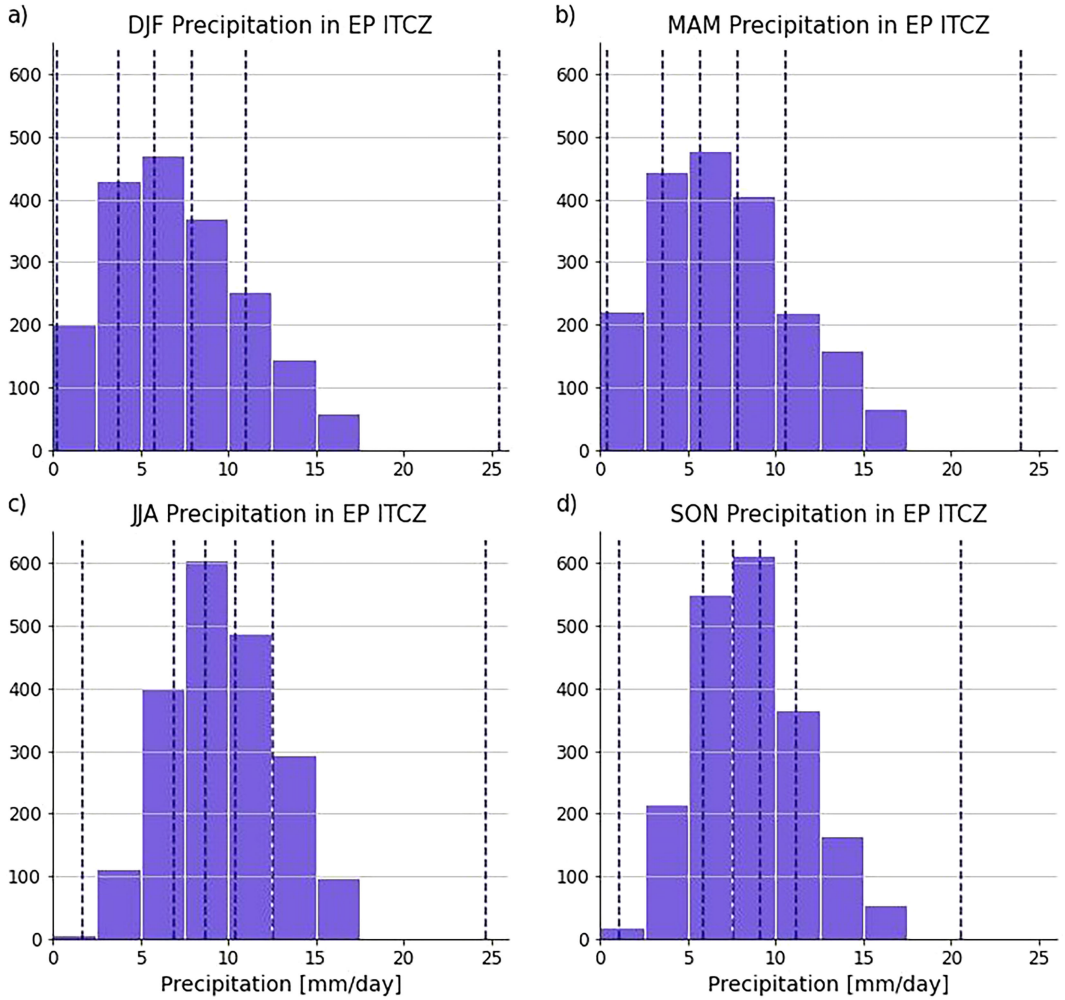

FIG. 2. Histograms of spatial averages of rainfall in the seasonally defined regions for (a) DJF, (b) MAM, (c) JJA, and (d) SON. The dashed lines represent the limits for the quantile binning (20th percentiles) used for the analysis.

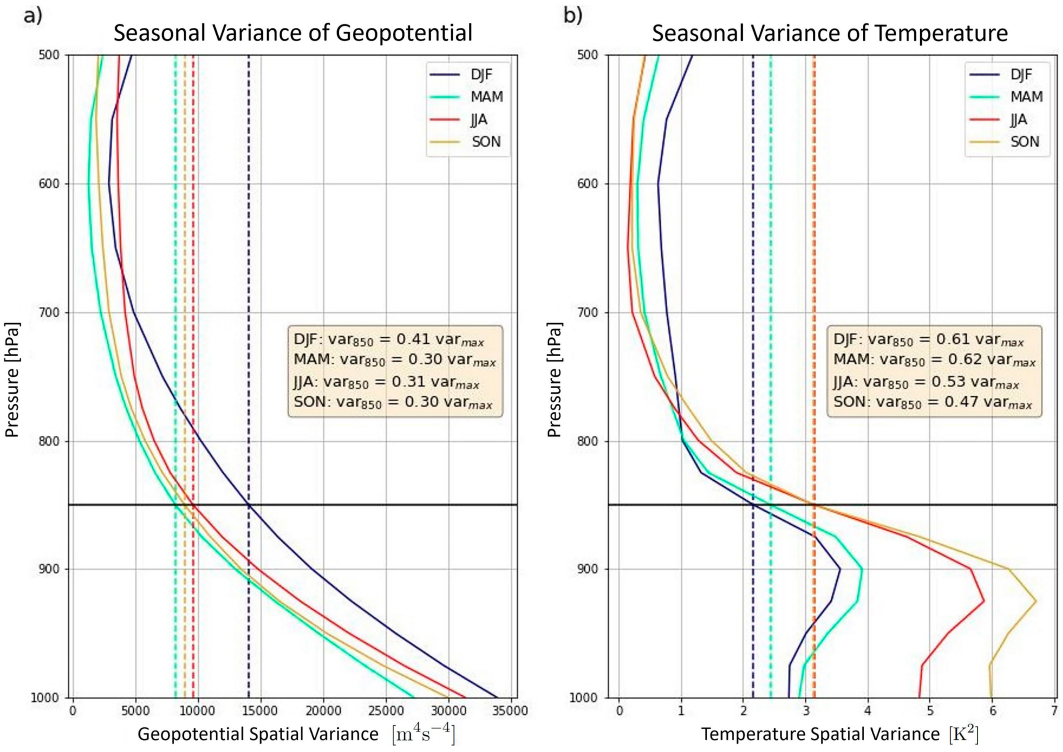

FIG. 3. (a) The vertical profile of total spatial variance of geopotential, calculated at each given pressure level for different seasons. (b) The total spatial variance of temperature calculated at each given pressure level for different seasons. These data come from a decade (2007–17) of ERA5 monthly averaged products over the eastern Pacific (20°S–20°N and 180°–80°W).

The 1000-hPa geopotential is separated into two components. The decomposition performed in this study is influenced by the decomposition applied previously in BB09a. These are the geopotential at the PBL top, $\Phi(p = p_{\text{top}})$, and the PBL thickness, or difference between geopotential at p_{top} and at 1000 hPa, denoted by $\Delta\Phi$:

$$\Phi(p = 1000 \text{ hPa}) = \Phi(p = p_{\text{top}}) - \Delta\Phi,$$

where p_{top} is the pressure level at the top of the PBL.

The most appropriate choice for the height of the PBL is determined empirically, based on the correlation between SST and temperature as a function of pressure (see section 3). Following the discussion above, we hypothesize that $\Delta\Phi$ is strongly determined by SST while $\Phi(p = p_{\text{top}})$ is more responsive to free-tropospheric dynamics. We composite both geopotential components on the precipitation quintiles, calculate anomalies from the mean, and examine how their spatial structures and the magnitudes of their spatial variations (over the domain 180°–70°W, 20°S–20°N) vary across the different rainfall quintiles.

3. Results

The spatial variances of the seasonal means of geopotential and temperature are plotted as functions of pressure in Fig. 3. Spatial variances are calculated over a region from 120° to 86°W and from 20°S to 20°N. This larger region is used as opposed to the smaller regions applied for the precipitation binning since this variance study is meant to gain greater insight into the large-scale characteristics of the tropical eastern Pacific. The spatial variance of Φ is greatest at the surface in every season. For almost every season, the variance of the geopotential at 850 hPa has decreased to roughly one-third of the total variance at the surface. The temperature variance maximizes around 900 hPa before declining rapidly, reaching a regime of much weaker temperature gradients above 800 hPa. We associate the relatively large temperature variance at the surface to the direct influence of SST variance, which is greater than that of atmospheric temperature due to the smaller radius of deformation in the ocean. We do not fully understand the maxima at 900 hPa but speculate that they may be due to undulations of the trade inversion, where one exists (i.e., over the parts of the domain with cooler SST). From this figure, we conclude that while no single level precisely defines a boundary between the PBL and the free troposphere in this spatially and temporally aggregated view, 850 hPa is a reasonable choice. We can also see that in the seasons spanning June to August (JJA) and September to November (SON), we have greater variance within the PBL than in the seasons between December and February (DJF) and March to May (MAM), associated with greater SST gradients

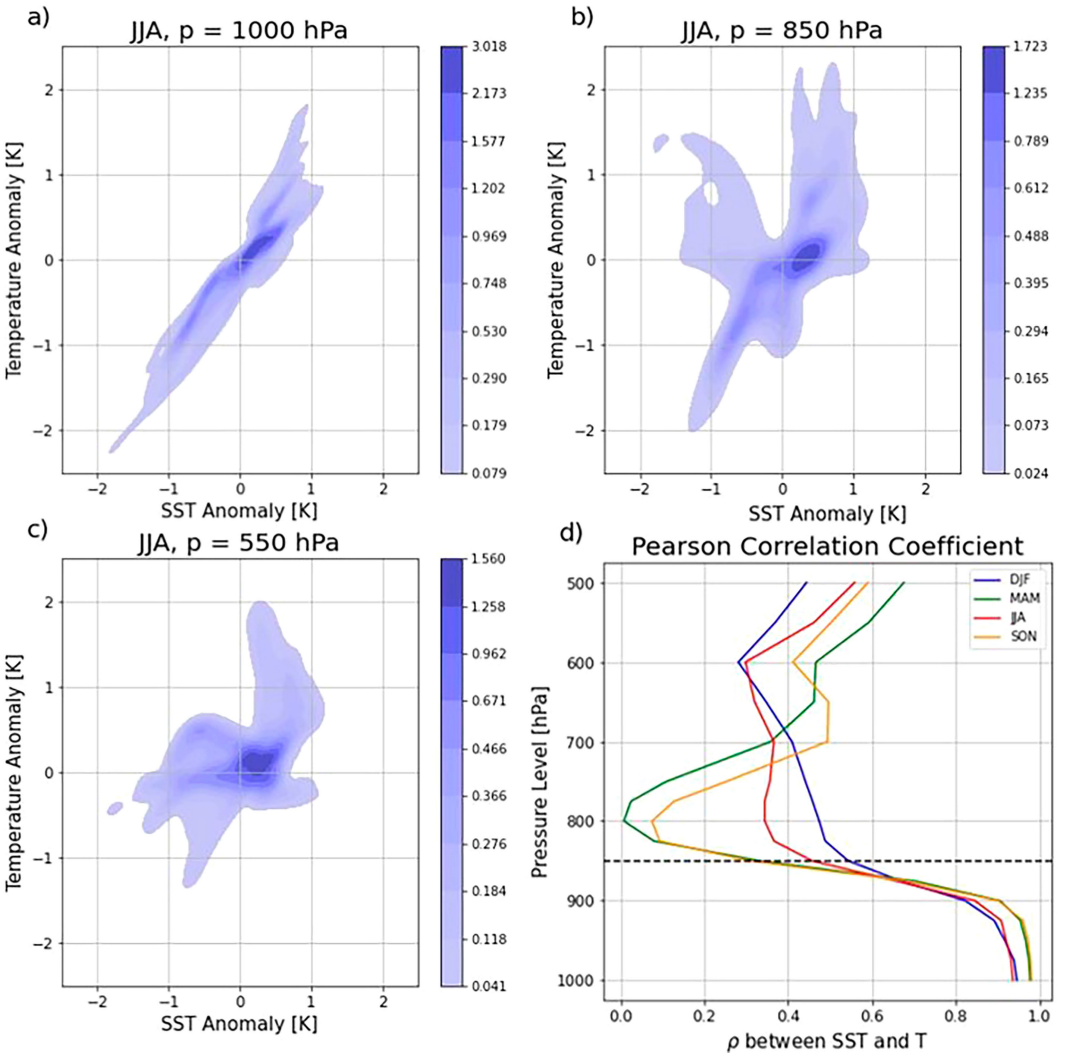

FIG. 4. (a)–(c) The joint probability distribution functions of seasonal JJA SST anomalies and corresponding temperature anomalies over the study domain at the levels 1000, 850, and 550 hPa, respectively, are displayed. (d) The calculated Pearson correlation coefficient between the two anomaly fields at various pressure levels.

during the northern summer and fall. For this reason, as well as because it is the season of strongest precipitation in the eastern Pacific ITCZ (and the time period of the OTREC2019 field program), we will focus on JJA for most of our analysis.

To further inform our choice of p_{top}, Fig. 4 shows the joint probability distribution functions of SST anomalies and the overlying air temperature anomalies during the JJA season at the (Fig. 4a) 1000-, (Fig. 4b) 850-, and (Fig. 4c) 550-hPa pressure levels from the ERA5 dataset. In Fig. 4d, we show the Pearson correlation coefficient between the two anomalies, ρ, as a function of pressure for all seasons. We can see in Fig. 4d that there is a strong positive correlation between SST and atmospheric temperature below 900 hPa, with $\rho > 0.9$, followed by a sharp decrease between 900 and 800 hPa, associated with increasing complexity of the joint probability distribution functions as pressure decreases, as exemplified in Figs. 4a–c. This figure further supports 850 hPa as a reasonable choice for p_{top}, particularly since we wish to define the PBL as that layer in which the atmospheric temperature is strongly controlled by the SST.

Based on the above analysis, we choose $p_{top} = 850$ hPa and construct composites of Φ_{850hPa} and $\Delta\Phi$—the components of 1000-hPa geopotential attributable to free-tropospheric geopotential and PBL thickness, respectively—indexed on daily ITCZ precipitation as described above. The high-pass-filtered composites for the driest and rainiest quintiles in JJA are shown in Fig. 5, superimposed on the corresponding precipitation composites themselves.

The dry and rainy composites in Φ_{850hPa} (Fig. 5) are similar in structure, but with opposite signs. The rainy composite shows an elongated low centered slightly north of the precipitation maximum and on its eastern side, with a broad high to the southwest extending well into the Southern Hemisphere, while the dry composite shows the mirror image. The composites on the intermediate precipitation bins show structures

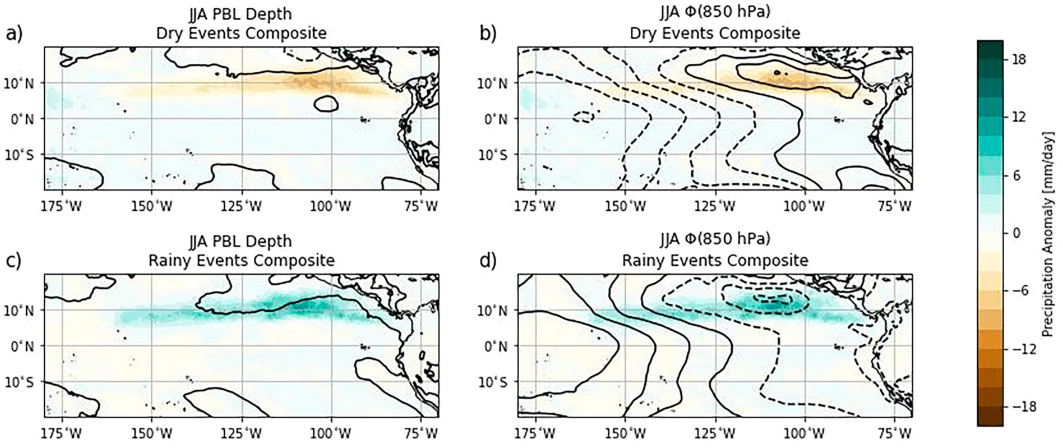

FIG. 5. The JJA daily geopotential component anomalies composited by daily precipitation quintiles. A high-pass filter has been applied to isolate subseasonal time scales as described in the text. (a),(c) The PBL depth anomalies for the driest and rainiest quintiles, respectively. (b),(d) The 850-hPa geopotential anomalies for the driest and rainiest quintiles, respectively. The contour interval for the geopotential anomalies is 10 $m^2\ s^{-2}$. The color shading indicates the composite precipitation anomalies associated with each quintile.

that transition smoothly and monotonically between these opposites (not shown). The composites in $\Delta\Phi$, meanwhile (Fig. 5), show much smaller anomalies.

To further quantify the relative magnitudes of variability in $\Delta\Phi$ and Φ_{850hPa} in a compact way, Fig. 6 shows the total spatial variances for the high-pass composites in all five rainfall quintiles and all four seasons. The variances in Φ_{850hPa} (crosses) are uniformly greater than those in $\Delta\Phi$ (circles) and generally much greater, particularly in the highest and lowest quintiles. This implies that while the 1000-hPa geopotential component that is directly related to the SST field (per LN87) remains nearly fixed as precipitation varies on subseasonal time scales, the same precipitation variations are associated with much larger variations in geopotential at the top of the PBL.

To understand the role of the high-pass filter in the above results, in Fig. 7, we present the same analysis without that filter, so that the composites include rainfall variations at all frequencies resolved in the data. The composites of Φ_{850hPa} are similar to those in Fig. 5, computed with the filter. The composites of $\Delta\Phi$, on the other hand, show greater amplitudes in the unfiltered data (Fig. 7), with an elongated low thickness to the north of the ITCZ in the dry composite and a high thickness there in the rainy composite, compared to the filtered composites (Fig. 5). Figure 8 shows the total spatial variance for each field across precipitation events in each season for the full signal, that is, the analog to Fig. 6 but without the high-pass filter. For JJA and SON, the total variance at 850 hPa varies drastically between different precipitation quintiles, while the variance within the PBL thickness remains nearly fixed, comparatively. However, the variance during DJF and MAM shows a different pattern: the total variance in the PBL thickness is higher for the dry and wet bins but is comparable or even exceeds the variance at 850 hPa.

The differences between Figs. 5 and 6 and Figs. 7 and 8 reflect the presence of low-frequency, i.e., seasonal-to-interannual, variability in the latter, while the former are purely subseasonal, as well as the interaction between the high and low frequencies. It is reasonable to assume that much of this low-frequency variability in atmospheric geopotential is associated with variability in

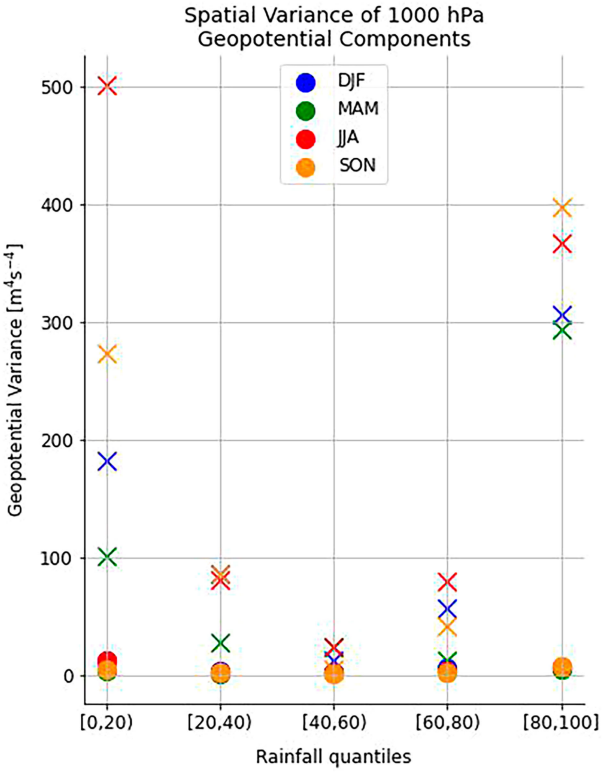

FIG. 6. Spatial variance of the subseasonal geopotential components. The spatial variances of the PBL depth are denoted by the circle marker, and the spatial variances of the 850-hPa geopotential are denoted by the × markers.

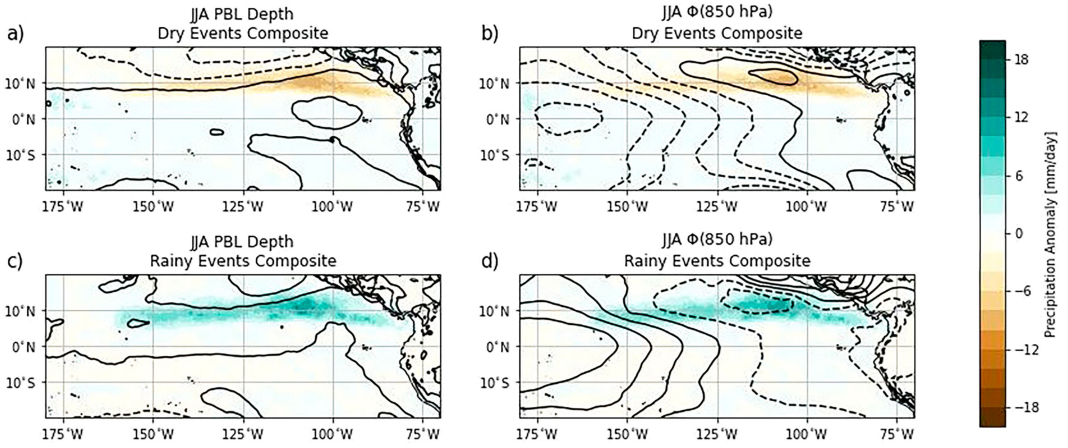

FIG. 7. As in Fig. 5, but without the high-pass filter, so that low frequencies are also included.

SST, including, e.g., ENSO and the Pacific meridional mode (PMM; Chiang and Vimont 2004). The relatively large variance in unfiltered $\Delta\Phi$ in DJF and MAM (Fig. 8) is consistent with this, since ENSO SST anomalies tend to be greatest in DJF while PMM SST anomalies tend to be greatest in MAM.

Our analysis here focuses on the geopotential, i.e., mass field, as this is most directly associated with SST in the PBL. The mass field is also directly related to the wind field, in both the free troposphere and the PBL, as discussed in the introduction. For completeness, we show JJA composites of high-pass-filtered, anomalous 100-m wind, 850-hPa geopotential level, and divergence for the highest and lowest precipitation quantiles in Figs. 9a and 9b, while Fig. 9c shows the mean 100-m winds and divergence. In the lowest precipitation quantile, there is anomalous divergence under the area of climatological low precipitation, with anomalous convergence to its south, and northerly wind anomalies connecting the two. This pattern monotonically transitions to reverse sign in the highest precipitation quintile, which is a confirmation of the relationship between low-level dynamics and precipitation. We do not further analyze the relationship between the mass and wind fields here, e.g., using a mixed-layer model as in past studies (e.g., Battisti et al. 1999; Chiang et al. 2001; Stevens et al. 2002; McGauley et al. 2004; Raymond et al. 2006; BB09a; Duffy et al. 2020). To do so would require consideration of downward momentum mixing as well as horizontal pressure gradients, Coriolis and frictional forces, and possibly nonlinear effects (Gonzalez et al. 2016).

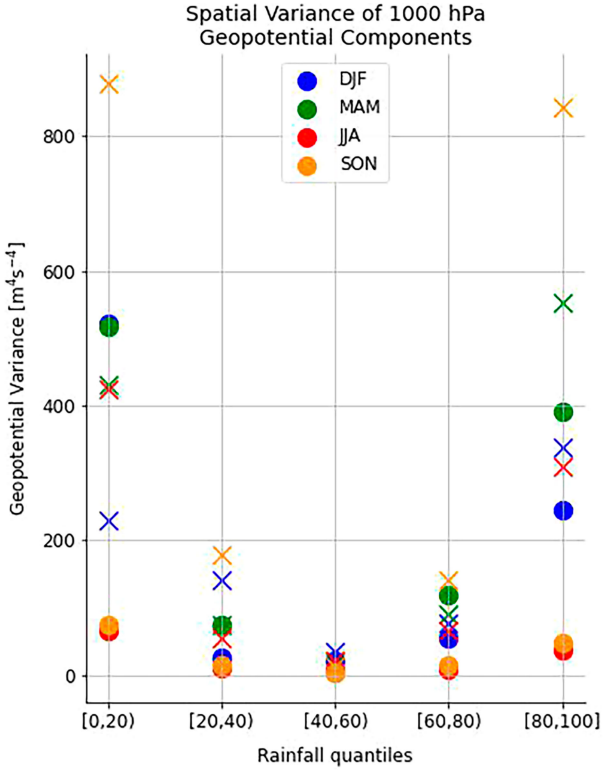

FIG. 8. As in Fig. 6, but without the high-pass filter, so that low frequencies are also included.

This analysis was performed for all seasons using various time steps and regions applied for the binning of TRMM data. All results are consistent with the conclusions presented in this work. A summary of different precipitation regions used and the spatial variance calculations are included in supplementary materials.

4. Conclusions

To understand the relationship of the mass and flow fields to precipitation variability in the region where the direct control by SST via PBL temperature is most important, we have presented an analysis of the geopotential variations associated with precipitation variability on daily time scales over the eastern Pacific ITCZ. We focus on the northern summer season, although some results are shown for all seasons. We decompose the 1000-hPa geopotential—approximately equivalent to surface pressure in geometric height coordinates—into a free-tropospheric component, represented by the geopotential at the top of the planetary boundary layer (PBL), and a PBL thickness component. Results are shown for data that have been high-pass-filtered to isolate subseasonal variability, as well as for the raw data, without any filtering. Our main findings are as follows.

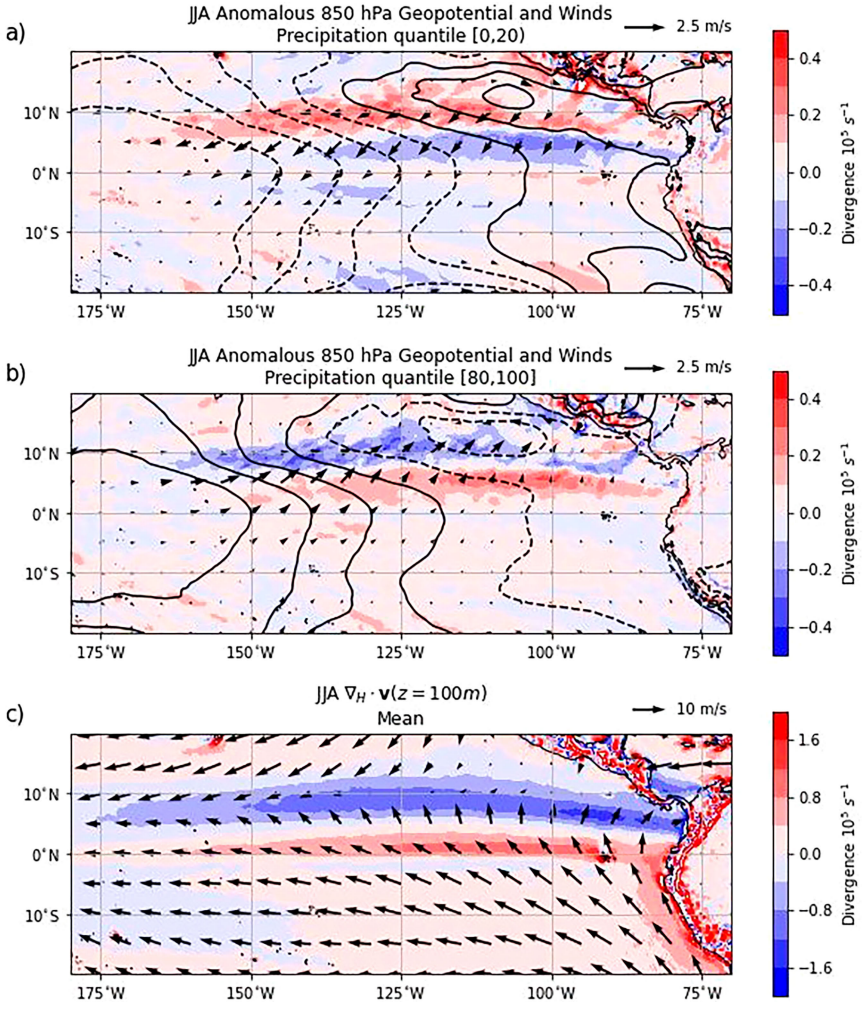

FIG. 9. (a),(b) The high-pass divergence and wind vector anomaly composites associated with the lowest and highest rainfall quintiles for the JJA season. The color contours represent the divergence composites, the contour lines represent the high-pass 850-hPa geopotential anomalies (plotted every 10 m^2 s^{-2}), and the vectors represent the anomalous wind vectors. (c) For comparison, the mean divergence pattern and the mean wind vector field are shown. Note the change of the vector scaling between the quintile composites and the mean.

The spatial variance in the geopotential and temperature fields in the region of interest decreases with height, especially sharp at around 800 hPa, as does the correlation between surface and air temperatures. We conclude that 850 hPa is a reasonable pressure level to indicate the top of the PBL for our purposes, and we use that choice in the rest of our analysis.

On subseasonal time scales (as isolated by the high-pass filter), the PBL thickness—the component of surface pressure associated directly with SST, via its control on PBL temperature—varies with precipitation almost not at all. The free-tropospheric mass field, on the other hand, varies much more strongly with precipitation on subseasonal time scales and imprints these variations on the surface pressure via the geopotential at 850 hPa.

When the data are not filtered, so that seasonal-to-interannual variations are retained, the PBL thickness shows greater variability than in the high-pass-filtered case, and in DJF, its magnitude even exceeds that of the free-tropospheric component. When creating quantiles of the filtered and nonfiltered SST dataset on rainfall, it becomes evident that this difference between the unfiltered and filtered results is associated with variability in SST (please see supplementary materials). This interpretation is consistent with the enhanced PBL thickness variability in DJF and MAM, when ENSO and the PMM—the main modes of SST variability—are most energetic.

These results support a view in which the component of the mass and flow fields associated directly with the SST, through its control on PBL temperature per LN87 and subsequent studies, can be considered approximately steady on subseasonal time scales. Meanwhile, ITCZ precipitation varies strongly in time on subseasonal time scales, and these variations are associated with relatively large variations in the free-tropospheric contribution to surface pressure. In other words, the PBL convergence

directly associated with sharp SST gradients can be considered an approximately steady forcing on the rest of the column, while free-tropospheric transients are associated with large fluctuations in precipitation. An interesting question is then how the steady SST-driven PBL convergence conditions the column and influences its response to those free-tropospheric transients. Single-column or small-domain cloud-resolving model experiments under parameterized large-scale dynamics, with PBL convergence either imposed [as in Bellon and Sobel (2010) or possible future extensions of their method], or simulated in response to imposed tropospheric temperature perturbations (Bernardez and Back 2022), could be one way to probe these interactions.

We have not attempted to untangle the causal relationship between the variations in precipitation and the mass field on subseasonal time scales. That is, to what extent are the geopotential variations shown in Figs. 5b and 5d causes of the associated precipitation variations, versus being caused by them? This is surely a difficult question to answer, as with many aspects of the interaction of convection and large-scale dynamics in the tropics, due to the tight coupling between them. Again numerical modeling is likely the best way to get at this question. Nor have we attempted to shed any new light on the details of the relationship between the mass and flow fields in the PBL. Many past studies have examined this (e.g., Battisti et al. 1999; Chiang et al. 2001; Stevens et al. 2002; McGauley et al. 2004; Raymond et al. 2006; BB09a; Duffy et al. 2020), and based on this, we take for granted that the mass field is a good indicator of the flow field and that our composites of 1000-hPa geopotential and surface wind and convergence together comprise a consistent picture. That said, there may well be subtleties in this relationship meriting further study as well.

Acknowledgments. This work was supported by National Science Foundation Grant AGS-1758603. We would like to acknowledge high-performance computing support from Cheyenne (DOI:10.5065/D6RX99HX) provided by NCAR's Computational and Information Systems Laboratory, sponsored by the National Science Foundation. We would also like to acknowledge OTREC2019 and all the brilliant scientists who participated in the campaign for inspiring this work. We also would like to thank the reviewers who dedicated their time and gave great insights over the work presented in this paper.

Data availability statement. Precipitation data (TRMM 3B42) are supplied by Goddard Earth Science Data and Information Services Center (GES DISC). Reanalysis products (ERA5) are accessible through Copernicus Climate Change Services (C3S) Climate Data Store (CDS). All programming applied for the analysis in this paper can be accessed via GitHub: https://github.com/ibunge96/geopotential_study.git.

REFERENCES

Back, L. E., and C. S. Bretherton, 2006: Geographic variability in the export of moist static energy and vertical motion profiles in the tropical Pacific. *Geophys. Res. Lett.*, **33**, L17810, https://doi.org/10.1029/2006GL026672.

——, and ——, 2009a: On the relationship between SST gradients, boundary layer winds, and convergence over the tropical oceans. *J. Climate*, **22**, 4182–4196, https://doi.org/10.1175/2009JCLI2392.1.

——, and ——, 2009b: A simple model of climatological rainfall and vertical motion patterns over the tropical oceans. *J. Climate*, **22**, 6477–6497, https://doi.org/10.1175/2009JCLI2393.1.

Battisti, D. S., E. S. Sarachik, and A. C. Hirst, 1999: A consistent model for the large-scale steady surface atmospheric circulation in the tropics. *J. Climate*, **12**, 2956–2964, https://doi.org/10.1175/1520-0442(1999)012<2956:ACMFTL>2.0.CO;2.

Bellon, G., and A. H. Sobel, 2010: Multiple equilibria of the Hadley circulation in an intermediate-complexity axisymmetric model. *J. Climate*, **23**, 1760–1778, https://doi.org/10.1175/2009JCLI3105.1.

Bernardez, M., and L. Back, 2022: On the controls of vertical motion top-heaviness. ESS Open Archive, https://doi.org/10.1002/essoar.10512628.1.

Bjerknes, J., 1969: Atmospheric teleconnections from the equatorial Pacific. *Mon. Wea. Rev.*, **97**, 163–172, https://doi.org/10.1175/1520-0493(1969)097<0163:ATFTEP>2.3.CO;2.

Chiang, J. C. H., and D. J. Vimont, 2004: Analogous Pacific and Atlantic meridional modes of tropical atmosphere–ocean variability. *J. Climate*, **17**, 4143–4158, https://doi.org/10.1175/JCLI4953.1.

——, S. E. Zebiak, and M. A. Cane, 2001: Relative roles of elevated heating and surface temperature gradients in driving anomalous surface winds over tropical oceans. *J. Atmos. Sci.*, **58**, 1371–1394, https://doi.org/10.1175/1520-0469(2001)058<1371:RROEHA>2.0.CO;2.

Daleu, C. L., and Coauthors, 2015: Intercomparison of methods of coupling between convection and large-scale circulation: 1. Comparison over uniform surface conditions. *J. Adv. Model. Earth Syst.*, **7**, 1576–1601, https://doi.org/10.1002/2015MS000468.

——, and Coauthors, 2016: Intercomparison of methods of coupling between convection and large-scale circulation: 2. Comparison over nonuniform surface conditions. *J. Adv. Model. Earth Syst.*, **8**, 387–405, https://doi.org/10.1002/2015MS000570.

Duffy, M. L., P. A. O'Gorman, and L. E. Back, 2020: Importance of Laplacian of low-level warming for the response of precipitation to climate change over tropical oceans. *J. Climate*, **33**, 4403–4417, https://doi.org/10.1175/JCLI-D-19-0365.1.

Fuchs-Stone, Ž., and Coauthors, 2020: OTREC2019: Convection over the east Pacific and southwest Caribbean. *Geophys. Res. Lett.*, **47**, e2020GL087564, https://doi.org/10.1029/2020GL087564.

Fueglistaler, S., and L. G. Silvers, 2021: The peculiar trajectory of global warming. *J. Geophys. Res. Atmos.*, **126**, e2020JD033629, https://doi.org/10.1029/2020JD033629.

Gill, A. E., 1980: Some simple solutions for heat-induced tropical circulation. *Quart. J. Roy. Meteor. Soc.*, **106**, 447–462, https://doi.org/10.1002/qj.49710644905.

Gonzalez, A. O., C. J. Slocum, R. K. Taft, and W. H. Schubert, 2016: Dynamics of the ITCZ boundary layer. *J. Atmos. Sci.*, **73**, 1577–1592, https://doi.org/10.1175/JAS-D-15-0298.1.

——, I. Ganguly, M. C. McGraw, and J. G. Larson, 2022: Rapid dynamical evolution of ITCZ events over the east Pacific. *J. Climate*, **35**, 1197–1213, https://doi.org/10.1175/JCLI-D-21-0216.1.

Held, I. M., and B. J. Hoskins, 1985: Large-scale eddies and the general circulation of the troposphere. *Advances in Geophysics*,

Vol. 28, Academic Press, 3–31, https://doi.org/10.1016/S0065-2687(08)60218-6.

Hersbach, H., and Coauthors, 2023a: ERA5 hourly data on pressure levels from 1940 to present. C3S CDS, accessed 15 January 2023, https://doi.org/10.24381/cds.6860a573.

——, and Coauthors, 2023b: ERA5 monthly averaged data on pressure levels from 1940 to present. C3S CDS, accessed 15 January 2023, https://doi.org/10.24381/cds.bd0915c6.

Huaman, L., C. Schumacher, and A. H. Sobel, 2022: Assessing the vertical velocity of the east Pacific ITCZ. *Geophys. Res. Lett.*, **49**, e2021GL096192, https://doi.org/10.1029/2021GL096192.

Lindzen, R. S., and S. Nigam, 1987: On the role of sea surface temperature gradients in forcing low-level winds and convergence in the tropics. *J. Atmos. Sci.*, **44**, 2418–2436, https://doi.org/10.1175/1520-0469(1987)044<2418:OTROSS>2.0.CO;2.

Lintner, B. R., G. Bellon, A. H. Sobel, D. Kim, and J. D. Neelin, 2012: Implementation of the Quasi-equilibrium Tropical Circulation Model 2 (QTCM2): Global simulations and convection sensitivity to free tropospheric moisture. *J. Adv. Model. Earth Syst.*, **4**, M12002, https://doi.org/10.1029/2012MS000174.

Matsuno, T., 1966: Quasi-geostrophic motions in the equatorial area. *J. Meteor. Soc. Japan*, **44**, 25–43, https://doi.org/10.2151/jmsj1965.44.1_25.

McGauley, M., C. Zhang, and N. A. Bond, 2004: Large-scale characteristics of the atmospheric boundary layer in the eastern Pacific cold tongue–ITCZ region. *J. Climate*, **17**, 3907–3920, https://doi.org/10.1175/1520-0442(2004)017<3907:LCOTAB>2.0.CO;2.

Neelin, J. D., 1989: On the interpretation of the Gill model. *J. Atmos. Sci.*, **46**, 2466–2468, https://doi.org/10.1175/1520-0469(1989)046<2466:OTIOTG>2.0.CO;2.

Raymond, D. J., C. S. Bretherton, and J. Molinari, 2006: Dynamics of the intertropical convergence zone of the east Pacific. *J. Atmos. Sci.*, **63**, 582–597, https://doi.org/10.1175/JAS3642.1.

Sobel, A. H., 2007: Simple models of ensemble-averaged tropical precipitation and surface wind, given the sea surface temperature. *The Global Circulation of the Atmosphere*, T. Schneider and A. H. Sobel, Eds., Princeton University Press, 219–251.

——, and C. S. Bretherton, 2000: Modeling tropical precipitation in a single column. *J. Climate*, **13**, 4378–4392, https://doi.org/10.1175/1520-0442(2000)013<4378:MTPIAS>2.0.CO;2.

——, and J. D. Neelin, 2006: The boundary layer contribution to intertropical convergence zones in the quasi-equilibrium tropical circulation model framework. *Theor. Comput. Fluid Dyn.*, **20**, 323–350, https://doi.org/10.1007/s00162-006-0033-y.

——, J. Nilsson, and L. M. Polvani, 2001: The weak temperature gradient approximation and balanced tropical moisture waves. *J. Atmos. Sci.*, **58**, 3650–3665, https://doi.org/10.1175/1520-0469(2001)058<3650:TWTGAA>2.0.CO;2.

——, I. M. Held, and C. S. Bretherton, 2002: The ENSO signal in tropical tropospheric temperature. *J. Climate*, **15**, 2702–2706, https://doi.org/10.1175/1520-0442(2002)015<2702:TESITT>2.0.CO;2.

Stevens, B., J. Duan, J. C. McWilliams, M. Münnich, and J. D. Neelin, 2002: Entrainment, Rayleigh friction, and boundary layer winds over the tropical Pacific. *J. Climate*, **15**, 30–44, https://doi.org/10.1175/1520-0442(2002)015<0030:ERFABL>2.0.CO;2.

Tropical Rainfall Measuring Mission, 2018: TRMM (TMPA) rainfall estimate L3 3 hour 0.25 degree × 0.25 degree, version 7. GES DISC, accessed 15 January 2023, https://doi.org/10.5067/TRMM/TMPA/3H/7.

Webster, P. J., 1972: Response of the tropical atmosphere to local, steady forcing. *Mon. Wea. Rev.*, **100**, 518–541, https://doi.org/10.1175/1520-0493(1972)100<0518:ROTTAT>2.3.CO;2.

Wu, Z., E. S. Sarachik, and D. S. Battisti, 1999: Thermally forced surface winds on an equatorial beta plane. *J. Atmos. Sci.*, **56**, 2029–2037, https://doi.org/10.1175/1520-0469(1999)056<2029:TFSWOA>2.0.CO;2.

Zhang, C., M. McGauley, and N. A. Bond, 2004: Shallow meridional circulation in the tropical eastern Pacific. *J. Climate*, **17**, 133–139, https://doi.org/10.1175/1520-0442(2004)017<0133:SMCITT>2.0.CO;2.